DOI: 10.1002/ejic.201100637

Oleum and Sulfuric Acid as Reaction Media: Structural Features and Thermal Behavior of $RE_2[W_2O_3(SO_4)_6]$ (RE = Sm–Gd, Ho), $RE_2Nb_2O_2(SO_4)_3[H(SO_4)_2]_2$ (RE = Y, Ce–Nd, Sm–Er), $Sm_2Nb_2O_2(SO_4)_5(S_2O_7)$, and $M_2Nb_4O_5(SO_4)_8$ (M = Bi, Eu)

Ulf Betke[a] and Mathias S. Wickleder*[a]

Keywords: Rare Earths / Niobium / Tungsten / Refractory metals / Sulfates / Thermal decomposition

The first examples of ternary sulfates containing refractory metals and trivalent ions of the rare-earth group and bismuth were prepared by solvothermal synthesis from H_2SO_4/SO_3 mixtures. The tungsten compounds $RE_2[W_2O_3(SO_4)_6]$ (RE = Sm–Gd, Ho) were obtained by the reaction of $WOCl_4$ and RE_2O_3 in oleum (25 % SO_3). They crystallize in the monoclinic space group *C*2/*c* and contain the unique $[W_2O_3(SO_4)_6]^{6-}$ anion. Thermal decomposition leads to the oxides $RE_2O(WO_4)_2$. Tetragonal rare-earth–niobium sulfates of the type $RE_2Nb_2O_2(SO_4)_3[H(SO_4)_2]_2$ (RE = Y, Ce–Nd, Sm–Er) (space group $P\bar{4}2_1m$) were synthesised from $NbCl_5$ and RE_2O_3 in 100 % H_2SO_4. They contain $[O_3SO{\cdots}H{\cdots}OSO_3]^{3-}$ ions featuring a strong hydrogen bond and form a polymeric structure with niobium in an octahedral coordination and the rare-earth ion is surrounded by eight $[SO_4]$ tetrahedra in the form of a square antiprism. The decomposition temperature of $RE_2Nb_2O_2(SO_4)_3[H(SO_4)_2]_2$ depends on the size of the respective rare-earth ion with a maximum in thermal stability found for RE = Sm–Gd (≈550 °C). The reaction of $NbCl_5$ and $Sm(NO_3)_3{\cdot}6H_2O$ in oleum (25 % SO_3) yielded $Sm_2Nb_2O_2(SO_4)_5(S_2O_7)$, which is a possible intermediate of the thermal decomposition of $Sm_2Nb_2O_2(SO_4)_3[H(SO_4)_2]_2$. It crystallizes in the monoclinic space group *I*2/*a* and contains $^2_\infty[NbO(SO_4)_{2/2}(SO_4)_{3/3}]$ layers connected by $^2_\infty[Sm(SO_4)_{2/4}(S_2O_7)_{2/4}]$ units to a polymeric structure. Reaction of $NbCl_5$ with $(BiO)_2CO_3$ or Eu_2O_3 in 95 % H_2SO_4 yielded $M_2Nb_4O_5(SO_4)_8$ (M = Bi, Eu, monoclinic, space group *C*2/*c*). These compounds contain the unprecedented $[M_2Nb_4O_5]^{16+}$ cluster cation and decompose into $MNbO_4$ and Nb_2O_5 on heating.

Introduction

The name "refractory metals" is commonly used for metals that are characterized by high melting and boiling points as well as distinctive chemical inertness from the formation of an oxidic passive layer. In engineering the refractory metals are mainly the elements niobium, tantalum, molybdenum, tungsten, and rhenium. All these metals form their most stable compounds in the highest possible oxidation state of +V to +VII. Nonetheless, a broad chemistry of substances containing low-valent refractory metals is known. In contrast to the large bulk of comprehensively characterized compounds of the refractory elements like chalcogenides, halogenides, coordination, and organometallic compounds in varying oxidation states the number of structurally characterized (particular binary) compounds containing complex oxo anions is astonishingly low.[1]

More is known about ternary refractory metal sulfates, whereupon the ternary component is usually limited to an alkaline metal ion. Examples are $MNbO(SO_4)_2$ (M = Rb, Cs, NH_4),[2] $Rb_2Mo_3O_9(SO_4)$,[3] $K_2MoO_2(SO_4)_2$,[4] and $Na_4MoO_2(SO_4)_3$.[5] They contain chains or layers of sulfate connected $[RMO_n]$ moieties (RM = refractory metal) that are networked to a three dimensional structure through alkaline metal ions. The structures of $K_4[MoO_2(SO_4)_3]$[6] and $M_8[W_2O_4(SO_4)_6]$ (M = K, Rb)[7,8] are different and contain discrete $[MoO_2(SO_4)_3]^{4-}$ and $[W_2O_4(SO_4)_6]^{8-}$ ions, respectively. In this context it is worth mentioning $K_7[M(SO_4)]$ (M = Nb, Ta)[9] and $K_3[Nb(SO_4)_4]$,[10] which contain the refractory metal in a homoleptic anionic complex without the terminal oxido ligands usually found for compounds of these elements. However, no ternary refractory metal sulfates are known with a di- or trivalent metal ion as the ternary component.

Since the binary refractory metal sulfates prepared in our group recently appeared to be precursors for the generation of the corresponding metal oxides,[11] we started to investigate ternary sulfates of these elements in order to generate new ternary oxidic phases by thermal decomposition. The focus has been on ternary refractory metal sulfates with rare-earth ions or ions similar to the rare-earth elements

[a] Carl von Ossietzky University of Oldenburg, Institute of Pure and Applied Chemistry,
Carl-von-Ossietzky Straße 9–11, 26129 Oldenburg, Germany
Fax: +49-441-798-3352
E-mail: mathias.wickleder@uni-oldenburg.de

Supporting information for this article is available on the WWW under http://dx.doi.org/10.1002/ejic.201100637.

 WILEY ONLINE LIBRARY © 2011 Wiley-VCH Verlag GmbH & Co. KGaA, Weinheim

(Bi^{3+}), as this substance class is not reported in the literature. In this work the crystal structures and thermal decomposition characteristics of new refractory metal sulfates with rare-earth elements and bismuth are presented.

Results and Discussion

Crystal Structures

$RE_2[W_2O_3(SO_4)_6]$ (RE = Sm–Gd, Ho) crystallizes in the monoclinic space group *C*2/*c* with four formula units in the unit cell. The asymmetric unit contains one tungsten atom, which has a distorted octahedral coordination with two oxido ligands and four monodentate sulfate ions (Figure 1). One oxido ligand (O11) is terminal, which is in good accord to the short W–O bond distance of around 168 pm, the other (O1) is a bridging oxido ion, which connects two [W=O] groups to a $[W_2O_3]$ moiety with a longer W–O bond distance of 190 pm. The oxido bridge is located on a twofold axis (site 4*e* of space group *C*2/*c*). The geometry of the $[W_2O_3]$ unit with an angle W1–O1–W1 of 147° and a torsion angle between both [W=O] moieties O11=W1···W1=O11 of 104° is comparable to other $[M_2O_3]$ fragments described in the literature, e.g. the $[V_2O_3]$ group in $V_2O_3(SO_4)_2$ (angle V–O–V: 148°, torsion angle O=V···V=O: 105°).[12] However, for phosphates of hexavalent transition metals exhibiting a $[M_2O_3]$ core, e.g. $Re_2O_3(PO_4)_2$ and orthorhombic $W_2O_3(PO_4)_2$, a similar angle M–O–M is found (Re: 161°, W: 145°),[13,14] but the M=O groups are not twisted against each other.

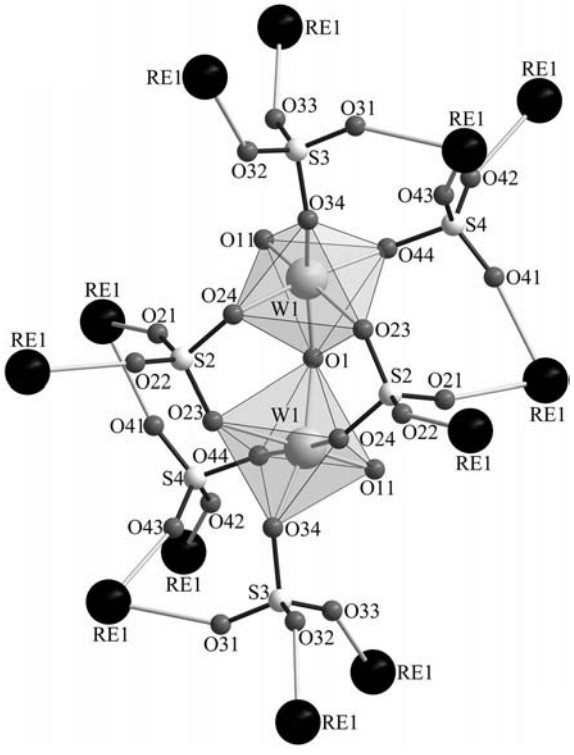

Figure 1. Atom labeling scheme for $RE_2[W_2O_3(SO_4)_6]$ (RE = Sm–Gd, Ho). Each W atom is surrounded octahedrally by one terminal oxido ligand (O11), four monodentate sulfato groups, and a bridging oxido ion (O1), so that finally a discrete $[W_2O_3(SO_4)_6]^{6-}$ unit is formed. Charge compensation is achieved by the incorporation of two RE^{3+} ions per formula unit.

The coordination sphere of the tungsten atoms in the $[W_2O_3]$ unit is completed by six sulfate tetrahedra. Two of them ([S2O$_4$]) bridge both W atoms and act as a chelating ligand towards the $[W_2O_3]$ moiety, but the other four sulfate ions ([S3O$_4$] and [S4O$_4$]) coordinate as monodentate ligands to only one tungsten atom, so that a discrete $[W_2O_3(SO_4)_6]^{6-}$ unit is finally formed. This new tungsten containing complex anion resembles the $[W_2O_4(SO_4)_6]^{8-}$ ion described in the literature,[7,8] i.e. with the same sulfate content or dimeric structure with respect to tungsten. However, the main difference is the lower number of oxido ligands; for the $[W_2O_4(SO_4)_6]^{8-}$ ion each tungsten atom carries two terminal oxido ligands lacking the bridging oxido ion. The distortion of the coordination polyhedron around tungsten in the $[W_2O_3(SO_4)_6]^{6-}$ unit becomes easily apparent in the elongation of the W–O23S2O$_3$ bond in the *trans* position to the terminal oxido ligand, which is significantly longer (225 pm) than the bonds to the sulfate tetrahedra coordinating *cis* to the [W=O] moiety (average 196 pm). The weaker coordination to W is reflected in the corresponding S2–O23 bond distance (147 pm), which is considerably shorter than the S–O bond distances of the [SO$_4$] oxygen atoms coordinating in a *cis* position to the terminal oxido ligand (154 pm on average).

In the crystal structure of $RE_2[W_2O_3(SO_4)_6]$ no connection of the $[W_2O_3(SO_4)_6]^{6-}$ ions through the sulfate tetrahedra takes place. Instead, the complex anions are stacked one upon each other along [010]. In this direction the $[W_2O_3(SO_4)_6]^{6-}$ group also exhibits a disorder, which leads to a splitting of the atom positions of the tungsten atom W1, the oxido bridge O1 and the terminal oxido ligand O11, so that formally the disordered $[W_2O_3(SO_4)_6]^{6-}$ moiety is created as a mirror image of the main site (Figure 2). However, the occupation of the disordered site ranges be-

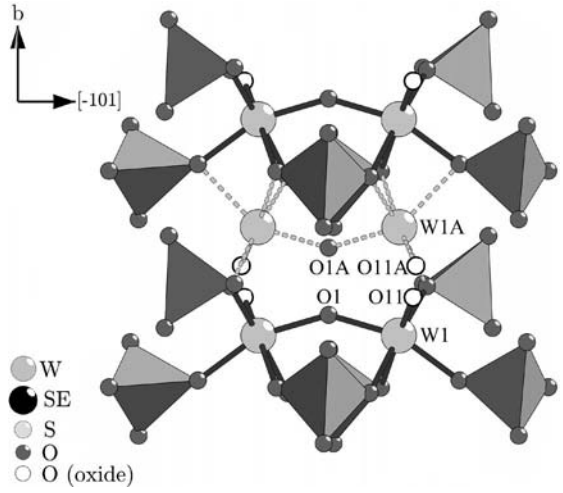

Figure 2. Disordered $[W_2O_3(SO_4)_6]^{6-}$ units along [010] in the crystal structure of $RE_2[W_2O_3(SO_4)_6]$ (RE = Sm–Gd, Ho). Formally, the disordered $[W_2O_3(SO_4)_6]^{6-}$ moiety (dashed light grey bonds) is created as mirror image of the main site (dark grey bonds).

 © 2011 Wiley-VCH Verlag GmbH & Co. KGaA, Weinheim

tween 6% (Eu) and 17% (Ho). In the [100] as well as the [001] direction the $[W_2O_3(SO_4)_6]^{6-}$ ions are networked through rare-earth cations, so that finally each sulfate tetrahedron is bonded to four metal atoms ([S2O$_4$]: 2 × W, 2 × RE; [S3O$_4$], and [S4O$_4$]: 1 × W, 3 × RE) (Figure 3). For the RE^{3+} ion a square antiprismatic coordination polyhedron is formed (Figure 4), where the average RE–O bond distance decreases from 240 pm for Sm^{3+} to 234 pm for Ho^{3+}. The weaker RE–O bond in comparison to the W–O bonds leads to shorter S–O bond distances for the respective [SO$_4$] oxygen atoms (average 144 pm).

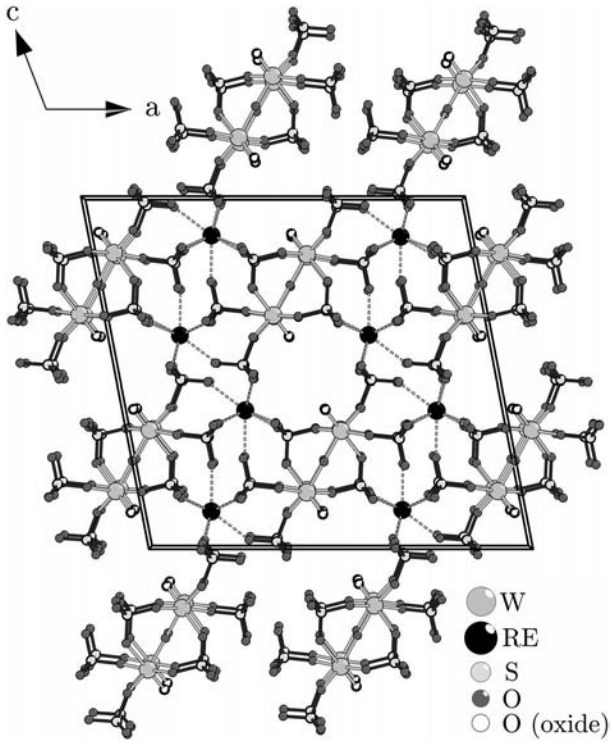

Figure 3. Structure of $RE_2[W_2O_3(SO_4)_6]$ (RE = Sm–Gd, Ho). The $[W_2O_3(SO_4)_6]^{6-}$ units are stacked one upon each other along [010]. In the [100] and [001] direction the complex anions are networked through RE^{3+} ions to give a polymeric structure.

$RE_2Nb_2O_2(SO_4)_3[H(SO_4)_2]_2$ (RE = Y, Ce–Nd, Sm–Er) crystallizes in the tetragonal space group $P\bar{4}2_1m$ with two formula units in the unit cell. The asymmetric unit contains one crystallographically distinguishable niobium atom as well as one rare-earth atom. For Nb a distorted octahedral coordination sphere through one oxido ligand (O1) and five monodentate sulfate tetrahedra is found (Figure 5). In contrast to other refractory metal oxide sulfates the oxido ligand is not terminal but coordinates to an adjacent rare-earth ion as well. This behavior is reflected in the Nb=O bond distance, which is slightly elongated (173 pm) compared to the distances usually found for a terminal oxido ligand [e.g. in $Nb_2O_2(SO_4)_3$: 169 pm].[11] The distances to the sulfate tetrahedra around Nb are unsuspicious with Nb–O bond distances ranging between 199 and 204 pm for the [SO$_4$] groups coordinating in a *cis* position to Nb=O and 213 to 216 pm for ligands *trans* to the oxido ligand.

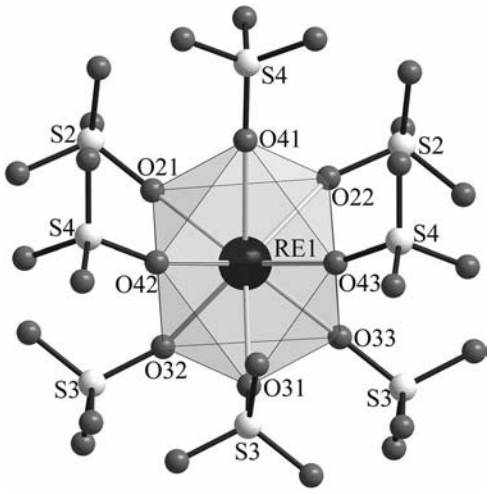

Figure 4. RE^{3+} ions in $RE_2[W_2O_3(SO_4)_6]$ (RE = Sm–Gd, Ho) surrounded by eight monodentate sulfato groups forming a square antiprismatic coordination polyhedron.

The lengthening of the Nb–O bond *trans* to the [Nb=O] moiety is less pronounced than in $Nb_2O_2(SO_4)_3$ (230 and 241 pm), because of the weaker Nb=O bond.

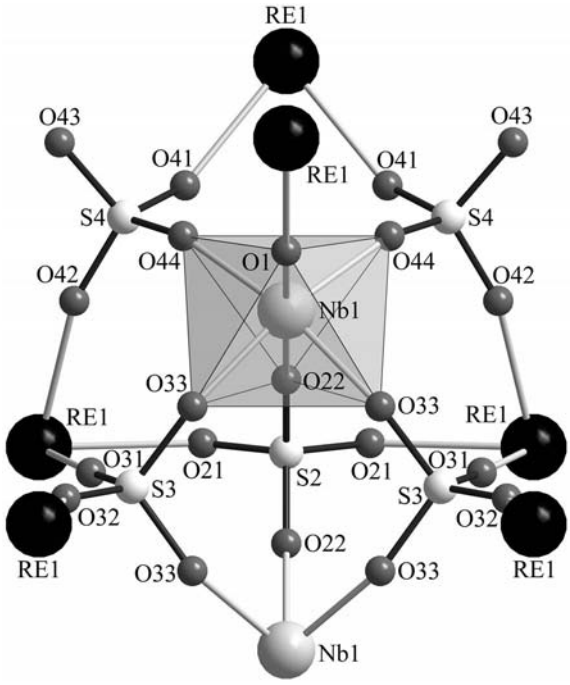

Figure 5. Atom labeling scheme for $RE_2Nb_2O_2(SO_4)_3[H(SO_4)_2]_2$ (RE = Y, Ce–Nd, Sm–Er). Each niobium atom is octahedrally surrounded by one oxido ligand (O1) and five monodentate [SO$_4$] tetrahedra. The oxido ligand is not terminal, but is bonded to an adjacent rare-earth ion.

Two of the five [SO$_4$] tetrahedra coordinating to Nb belong to a hydrogen bis(sulfate) ion, which is represented by the sulfur atom S4. The $[O_3SO\cdots H\cdots OSO_3]^{3-}$ ions are located on the $\bar{4}$ axis of space group $P\bar{4}2_1m$ and exhibit a strong hydrogen bond (O43···H···O43). The distance of the hydrogen bond between both sulfate tetrahedra is correlated with the radius of the rare-earth ion in the respective

 © 2011 Wiley-VCH Verlag GmbH & Co. KGaA, Weinheim

compound and varies between 252 pm (RE = Ce) and 244 pm (RE = Er). The corresponding S4–O43 (148 pm) bond distance lies between a noncoordinating S–O group and a S–OH unit (e.g. in H_2SO_4: 143 and 154 pm).[15] The geometry of the hydrogen bis(sulfate) ion in $RE_2Nb_2O_2(SO_4)_3[H(SO_4)_2]_2$ is in good accord with values reported in the literature, e.g. for $Rb_3[H(SO_4)_2]$ (distance of the O···O hydrogen bond: 249 pm, distance of S–OH···O: 154 pm).[16]

Each $[O_3SO{\cdots}H{\cdots}OSO_3]^{3-}$ ion binds to two niobium atoms as well as two rare-earth ions. The $[S2O_4]$ ion is located at a special site (2*c* of space group $P\bar{4}2_1m$, twofold axis/diagonal mirror planes) and coordinates two niobium and two rare-earth ions. The sulfato group $[S3O_4]$ binds to two Nb as well as two RE atoms. The S–O bond distances in the $[SO_4]$ tetrahedra reflect the different strengths of coordination to Nb and RE^{3+}. For S–O groups coordinating to a rare-earth cation (O21, O31/32, O41/42) an average distance of 144 pm is found. For S–O moieties binding to niobium a slight difference between coordination in a *trans* position to the oxido ligand (O22, average 148 pm) and bonding *cis* to the [Nb=O] moiety (O33, O44, average 150 pm) can be observed. For the RE^{3+} ions a square antiprismatic coordination sphere arises built up of eight monodentate $[SO_4]$ tetrahedra (Figure 6). The distances RE–O decrease with decreasing size of RE^{3+} from an average of 247 pm for Ce^{3+} to 233 pm found for the respective erbium compound.

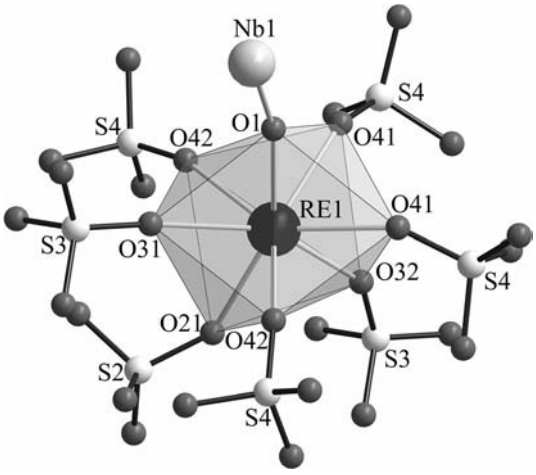

Figure 6. Rare earth cations in $RE_2Nb_2O_2(SO_4)_3[H(SO_4)_2]_2$ (RE = Y, Ce–Nd, Sm–Er) surrounded by eight monodentate sulfate tetrahedra forming a square antiprism.

Finally a polymeric structure is formed that consists of [Nb=O···RE] fragments. Two of these building units are connected by a $[S2O_4]$ ion, where the coordination takes place *trans* to the oxido ligand. Additionally, these [RE···O=Nb–OS2O$_2$–O–Nb=O···RE] arrangements are bridged by two $[S3O_4]$ ions coordinating both niobium atoms. The center of the $[RE_2Nb_2O_2(SO_4)_3]$ groups represented by the $[S2O_4]$ ion resides on the twofold axis of space group $P\bar{4}2_1m$ at [0 1/2 *z*] and [1/2 0 *z*], so that stacks along [001] are finally formed. All remaining coordination sites of niobium as well as the rare-earth ions are filled by the hydrogen bis(sulfate) ions, which are also stacked along the crystallographic *c* axis at [0 0 *z*] and [1/2 1/2 *z*] (Figure 7).

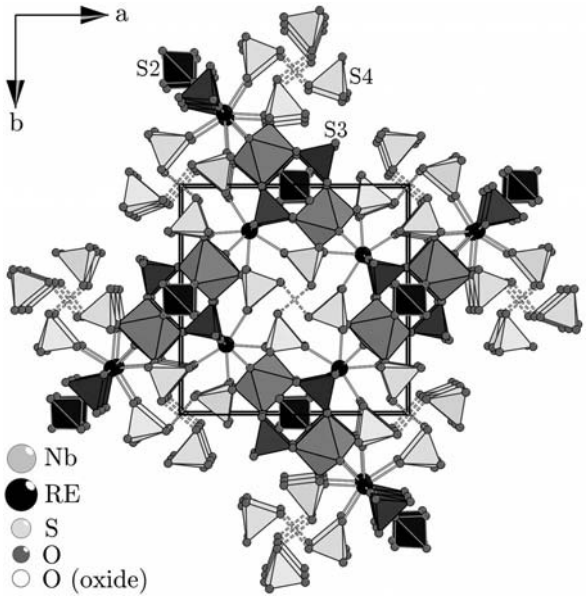

Figure 7. Polymeric structure of $RE_2Nb_2O_2(SO_4)_3[H(SO_4)_2]_2$ (RE = Y, Ce–Nd, Sm–Er) consisting of [Nb=O···RE] fragments connected by $[S2O_4]$ ions (black) flanked by $[S3O_4]$ tetrahedra (dark grey). These $[RE_2Nb_2O_2(SO_4)_3]$ groups are stacked along [001] and finally networked by hydrogen bis(sulfate) ions (light grey), exhibiting a strong hydrogen bond (dashed line).

$Sm_2Nb_2O_2(SO_4)_5(S_2O_7)$ crystallizes in the monoclinic space group *I*2/*a* with four formula units per unit cell. The asymmetric unit contains one niobium as well as one samarium atom. For niobium an octahedral coordination sphere built up of one terminal oxido ligand (O11) and five monodentate sulfato groups is found (Figure 8). In contrast to $RE_2Nb_2O_2(SO_4)_3[H(SO_4)_2]_2$ the oxido ligand is terminal and does not connect the Nb atom with adjacent rare-earth ions. This is easily reflected in the shorter bond length of 168 pm for Nb–O. The remaining Nb–O bond lengths range between 203 and 207 pm for the sulfate tetrahedra coordinating in the *cis* position to the [Nb=O] moiety, whereas for the bond *trans* to the oxido ligand a distinct elongation to 229 pm is found.

The crystal structure of $Sm_2Nb_2O_2(SO_4)_5(S_2O_7)$ exhibits three crystallographically distinguishable sulfato groups represented by the sulfur atoms S2, S4, and S5, as well as one disulfate group (S3). All oxygen atoms of each oxo anion coordinate to niobium or samarium, whereupon there are remarkable differences between the respective anions. First of all, the sulfato groups $[S4O_4]$ and $[S5O_4]$ connect the [Nb=O] moieties to double layers parallel to (001) at $a = 0.25$ and 0.75. According to the Niggli formula $^2_\infty[NbO(S4O_4)_{2/2}(S5O_4)_{3/3}]$, the oxo anions differ in their coordination of Nb as $[S4O_4]$ binds two niobium atoms utilizing the oxygen atoms O43 and O44, but $[S5O_4]$ tethers three refractory metals over O52, O53, and O54 (Figure 9). The terminal oxido ligands on niobium are oriented towards the layer surface in the [001] and [00–1] directions. The forma-

 © 2011 Wiley-VCH Verlag GmbH & Co. KGaA, Weinheim

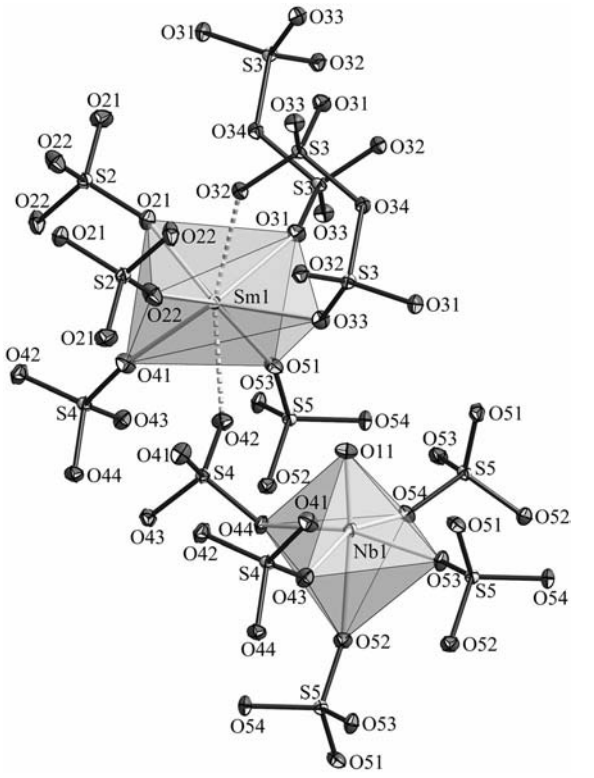

Figure 8. Atom labeling scheme and coordination polyhedra around Nb and Sm for $Sm_2Nb_2O_2(SO_4)_5(S_2O_7)$. The thermal ellipsoids are drawn at a 50% probability level. Niobium is octahedrally surrounded by one terminal oxido ligand (O11) and five monodentate sulfate tetrahedra. For Sm^{3+} a bicapped trigonal prism is found, which is built up of five monodentate $[SO_4]$ ions, one monodentate $[S_2O_7]$ group and one chelating $[S_2O_7]$ ion.

tion of layered structures is not unknown for oxide sulfates of high-valent metals and has also been found for $WO(SO_4)_2$, $Re_2O_5(SO_4)_2$, and $MoO(HSO_4)(SO_4)$.[11]

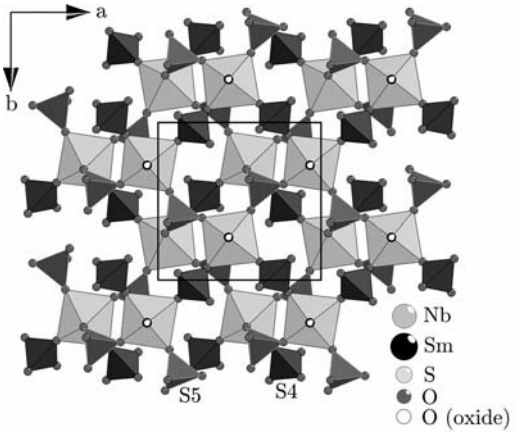

Figure 9. Layers of the formal composition $[NbO(SO_4)_2]$ in the crystal structure of $Sm_2Nb_2O_2(SO_4)_5(S_2O_7)$. The [Nb=O] moieties are networked to parallel double layers (001) through the sulfate ions $[S4O_4]$ (grey) and $[S5O_4]$ (dark grey). The formal composition of the layers is $^{1}_{\infty}[NbO(S4O_4)_{2/2}(S5O_4)_{3/3}]$ according to Niggli's formalism, therefore each niobium atom carries one negative charge.

However, according to the formal layer composition of $[NbO(SO_4)_2]$, each niobium atom carries one negative charge. This is compensated by the inclusion of layers with the formal composition $[Sm_2(SO_4)(S_2O_7)]$, which run parallel to (001) at $a = 0$ and 0.5 (Figure 10). These layers are built by connecting four Sm^{3+} cations through one $[S2O_4]$ group, furthermore each rare-earth ion is coordinated by one chelating and one monodentate disulfate ion. Therefore the $[S_2O_7]$ ion connects at least four different samarium ions according to the Niggli formula $^{2}_{\infty}[Sm(S2O_4)_{2/4}(S3_2O_7)_{2/4}]$. The connection between rare-earth and niobium containing layers is realized by the $[S4O_4]$ and $[S5O_4]$ tetrahedra using the oxygen atoms O41, O42, and O51, which are not coordinated to Nb resulting in a bicapped trigonal prism around Sm^{3+}.

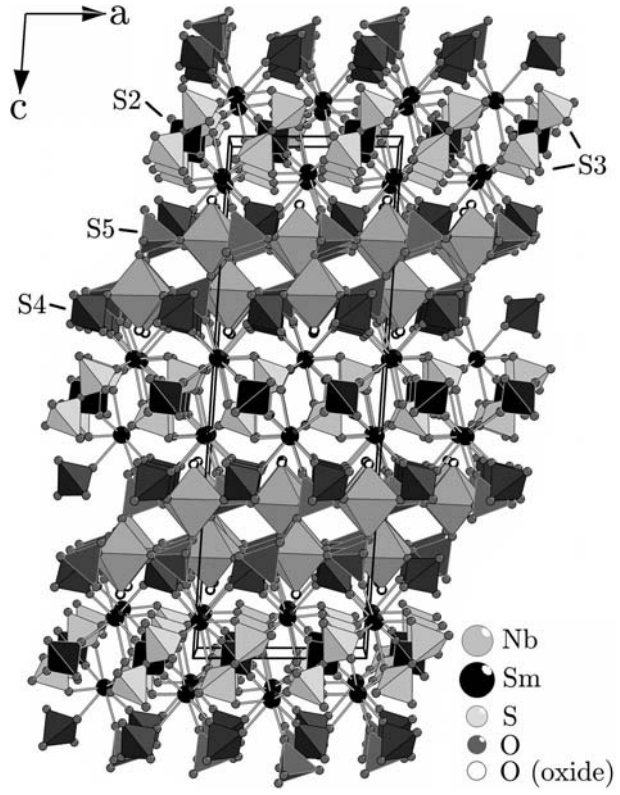

Figure 10. Crystal structure of $Sm_2Nb_2O_2(SO_4)_5(S_2O_7)$ built by the inclusion of $^{2}_{\infty}[Sm(S2O_4)_{2/4}(S3_2O_7)_{2/4}]$ layers as charge compensation between the $^{2}_{\infty}[NbO(S4O_4)_{2/2}(S5O_4)_{3/3}]$ layers.

$M_2Nb_4O_5(SO_4)_8$ (M = Bi, Eu) crystallizes in the monoclinic space group *C*2/*c* with 16 formula units per unit cell. The asymmetric unit contains at least eight niobium atoms as well as four M^{3+} cations. Four niobium atoms (Nb11, Nb22, Nb31, Nb41) are surrounded by one oxido ligand and one chelating sulfate ion and four monodentate sulfate tetrahedra forming a pentagonal bipyramid. For the remaining Nb atoms Nb12, Nb21, Nb32, and Nb42 an octahedral coordination through two oxido ligands and four monodentate sulfate ions is found. None of the oxido ligands is terminal, as O1B, O2B, O4B, O5B, O7B, O8B, O10B, and O11B connect niobium atoms with an adjacent M^{3+} cation, and O3B, O6B, and O9B bridge two niobium

 © 2011 Wiley-VCH Verlag GmbH & Co. KGaA, Weinheim

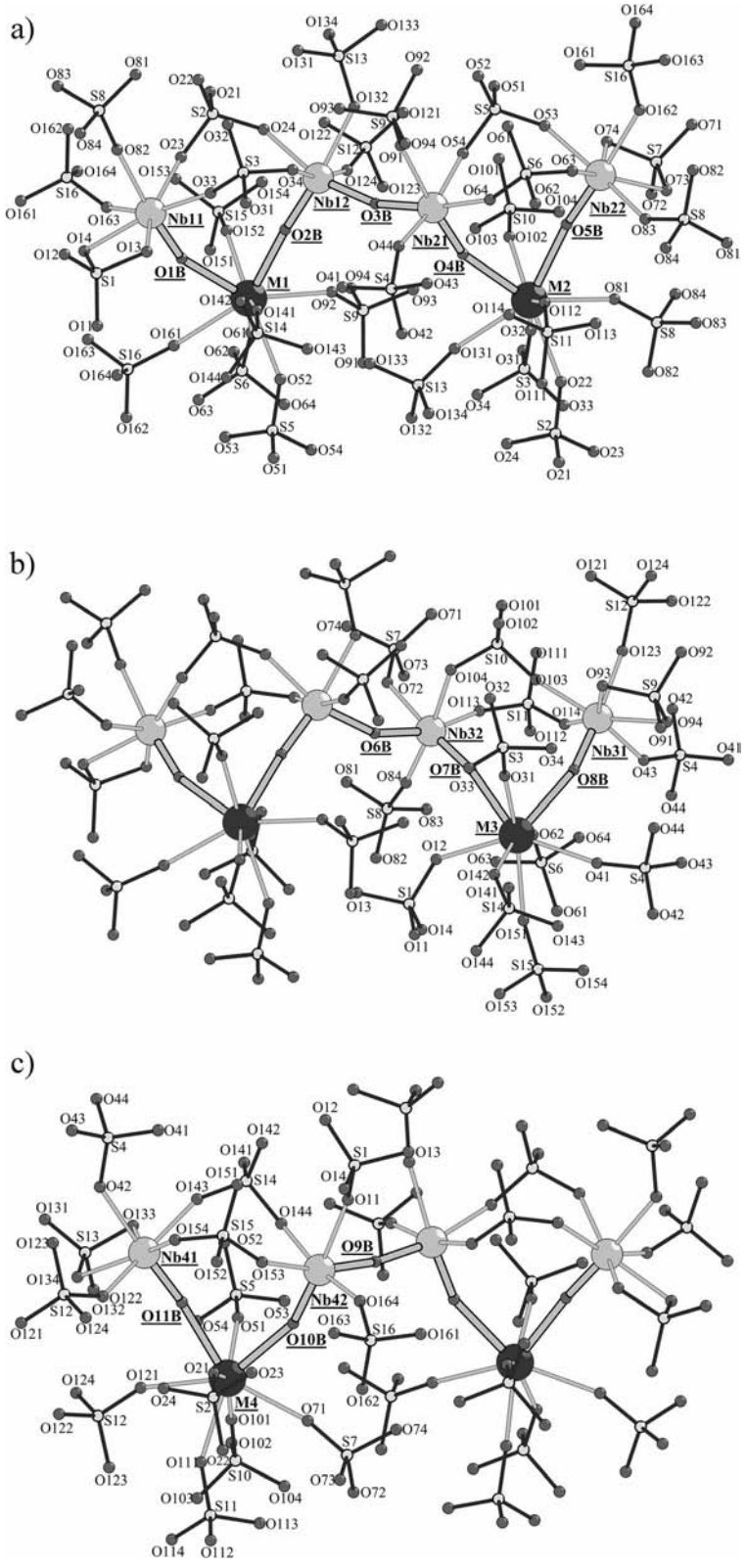

Figure 11. Three crystallographically distuingishable $[M_2Nb_4O_5]^{16+}$ cluster ions in the crystal structure of $M_2Nb_4O_5(SO_4)_8$ (M = Bi, Eu). Each consists of a [O=Nb–O–Nb=O] moiety featuring a linear Nb–O–Nb bridge, which is connected with two M^{3+} cations by an asymmetric M···O=Nb bond. Finally each M^{3+} ion is bonded to a further niobium atom, so that discrete $[M_2Nb_4O_5]^{16+}$ cluster ions are the result. The difference between the three cluster ions is their symmetry; cluster (a) is located on a screw axis, which runs through the central oxido bridge (O3B), and clusters (b) and (c) both reside on a twofold rotation axis with their central oxido bridge (O6B, O9B) on the special site 4*e*. The coordination sphere of all metal atoms is completed by sulfate tetrahedra, so for both central Nb atoms of each cluster an octahedral coordination sphere is found, whereas the outer Nb atoms exhibit a pentagonal bipyramidal coordination. The M^{3+} cation is surrounded by a square antiprism.

 © 2011 Wiley-VCH Verlag GmbH & Co. KGaA, Weinheim

atoms. However, a differentiation should be made between the nearly linear Nb–O–Nb bridges (average distance of Nb–O: 189 pm) and the highly asymmetric M–O–Nb bridges (average distance of Nb–O: 172 pm, average distance of M–O: 242 pm), which should rather be as M···O=Nb. However, no polymeric metal–oxide network is formed, as each [O=Nb–O–Nb=O] moiety connects only two M^{3+} ions, which are again coordinated through one [Nb=O] fragment each. Therefore a cluster cation of the composition $[M_2Nb_4O_5]^{16+}$ is formed, which roughly adopts the shape of a "W" with the Nb–O–Nb bridge located at the middle apex and M^{3+} at both lower ends (Figure 11). The remaining coordination sites of Nb and M^{3+} are filled with sulfate ions, resulting in an octahedral coordination sphere for both central Nb atoms, a square antiprism around M^{3+} and a pentagonal bipyramid around the outer Nb atoms. Finally the crystal structure is built by networking the $[M_2Nb_4O_5]^{16+}$ cluster cations through 16 crystallographically distinguishable sulfate tetrahedra to a polymeric structure (Figures 12 and 13). The large unit cell of this class of compounds can be explained by the fact that three different types of cluster cations exist. The first cluster [cluster (a)] in Figure 12 is located with the central oxido bridge (O3B) on a screw axis, whereas the cluster ions (b) and (c) reside on a twofold axis (oxido bridges O6B and O9B on site 4*e* of space group *C*2/*c*).

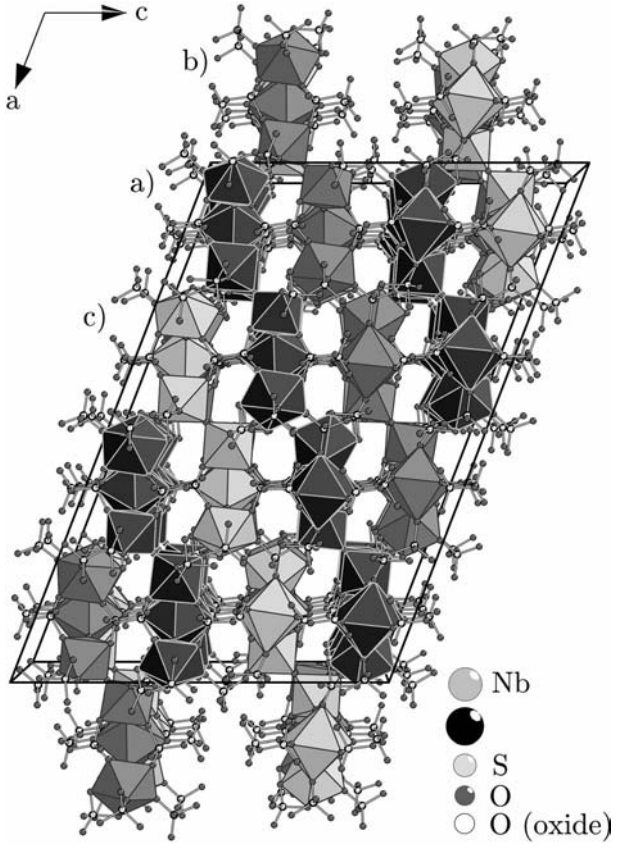

Figure 12. Structure of $M_2Nb_4O_5(SO_4)_8$ (M = Bi, Eu). The $[M_2Nb_4O_5]^{16+}$ cluster cations in are connected through $[SO_4]$ ions to form a polymeric structure. The cluster ions are stacked one upon each other along [010], whereas cluster (a) (dark grey) resides with its central oxido bridge on a screw axis, and clusters (b) (grey) and (c) (light grey) are located on a twofold axis.

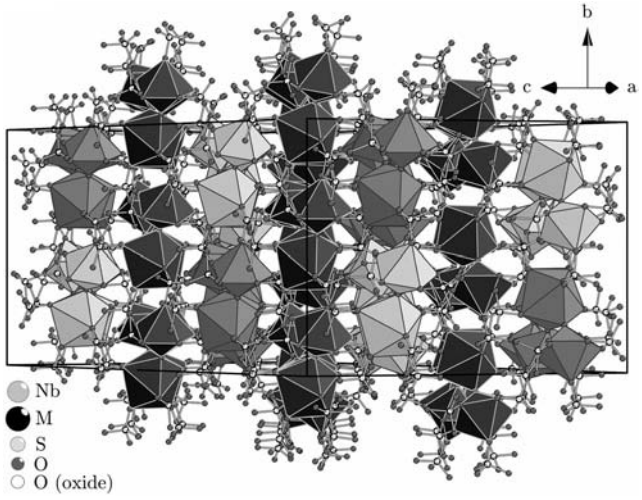

Figure 13. Strings formed by stacking the $[M_2Nb_4O_5]^{16+}$ cluster ions of $M_2Nb_4O_5(SO_4)_8$ (M = Bi, Eu) along [010]. The strings can be separated into two different classes: The first is formed by cluster ions of the type (a) exclusively (dark grey), the second is an alternating series of clusters (b) and (c) (grey and light grey, respectively).

Thermal Decomposition

$Eu_2[W_2O_3(SO_4)_6]$ decomposes in five steps, which are visible in the DTG curve, but the last two steps are not well separated. The first decomposition step should be considered as vaporisation of adherent sulfuric acid, which is completed at roughly 300 °C. The dry $Eu_2[W_2O_3(SO_4)_6]$ is thermally stable up to 340 °C. A molecule of SO_3 is split off between 340 °C and 405 °C. The observed and calculated loss of mass is in good accord with the loss of SO_3 (exp. 6.3%, calcd. 6.2%), and the decomposition product is most likely to be an oxide richer sulfate of the constitution $Eu_2W_2O_4(SO_4)_5$. On further heating this species disintegrates at 543 °C under the loss of two molecules of SO_3 into a species of the formal composition $Eu_2W_2O_6(SO_4)_3$, which is completed at 643 °C (exp. 19.5%, calcd. 18.5%).

For the simple tungsten sulfate $WO(SO_4)_2$ a decomposition into sulfur trioxide and WO_3 has been reported to occur up to 530 °C,[11] therefore the intermediate species $Eu_2W_2O_6(SO_4)_3$ should rather be considered as a mixture of $Eu_2(SO_4)_3$ and $2WO_3$. On further heating, two poorly separated steps can be observed in the TG curve, beginning at roughly 700 °C. In combination they can be assigned to the loss of three molecules of SO_3 according to the loss of mass (exp. 39.6%, calcd. 37.0%). This process is finished at 943 °C.

The final decomposition product of $Eu_2[W_2O_3(SO_4)_6]$ has been investigated by means of powder diffraction and infrared spectroscopy. Unfortunately the sample was shown to be amorphous towards X-rays, but from the IR spectrum

 © 2011 Wiley-VCH Verlag GmbH & Co. KGaA, Weinheim

the presence of sulfate can be eliminated because of the absence of the characteristic [SO_4] bands. A possibility is the formation of a phase with the composition $Eu_2W_2O_9$, which is known for RE = La and Pr and contains W and Eu in an equimolar ratio.[17,18]

$RE_2Nb_2O_2(SO_4)_3[H(SO_4)_2]_2$ (RE = Ce–Nd, Sm, Gd, Dy, Er) shows a rather interesting thermal behavior. All compounds exhibit a three or four step decomposition mechanism, and for the complete series the respective rare-earth niobates $RENbO_4$ (RE = Ce–Nd, Sm, Gd, Dy, Er) are formed as product. They have been identified by means of X-ray powder diffraction. The end temperature of the thermal decomposition lies in the narrow range between 900 and 980 °C, but the decomposition starting temperature and the decomposition pathways are highly correlated to the radius of the respective rare-earth ion. Initially, the decomposition temperature increases from 293 °C for the cerium compound up to 573 °C for the respective samarium analog. With decreasing radius of the rare-earth ion the decomposition temperature drops again to 415 °C for the erbium compound. Furthermore, four different decomposition pathways can be distinguished. The influence of the radius of RE^{3+} on the decomposition temperature and the decomposition pathway is illustrated in Figure 14.

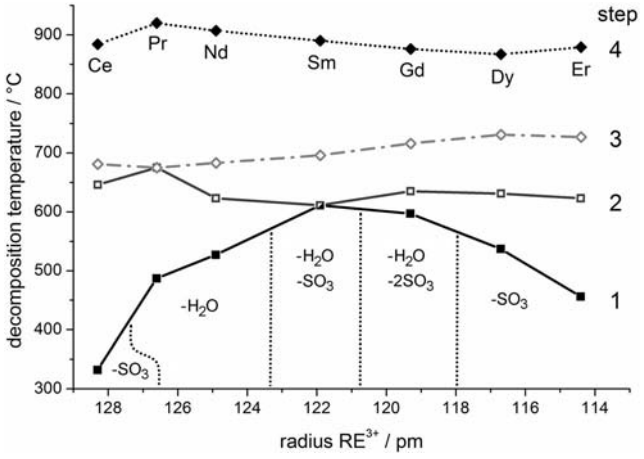

Figure 14. Starting temperatures for each decomposition step in the thermal decomposition of $RE_2Nb_2O_2(SO_4)_3[H(SO_4)_2]_2$ (RE = Ce–Nd, Sm, Gd, Dy, Er) in dependence of the respective RE^{3+} ionic radius (for eightfold coordination[19]). The starting temperatures of steps 2–4 are barely correlated to the radius of the rare-earth ion. For the first step the decomposition starting temperature increases from 293 °C for RE = Ce to a maximum of 573 °C for RE = Sm, and decreases again to 415 °C for RE = Er. Furthermore, the decomposition pathway depends on the radius of the rare-earth ion.

For the larger RE^{3+} ions of Pr and Nd the decomposition starts with the loss of a water molecule. The formation of a disulfate of the composition $RE_2Nb_2O_2(SO_4)_5(S_2O_7)$ as an intermediate is most likely. The loss of H_2O as an initial step can be understood comparatively well by looking at the hydrogen bond strength in the respective hydrogen bis(sulfate) ion. For the bigger rare-earth ions the distance between both sulfate tetrahedra is larger, therefore the hydrogen atom is bonded less strongly, so the dehydration is most favorable in this case. However, the increase in the hydrogen bond strength from the Pr compound towards the Nd homologue is reflected in the increase of the decomposition temperature (Pr: 461 °C, Nd: 500 °C). On further heating sulfur trioxide is given off in at least two steps (first $4 \times SO_3$ at ca. 680 °C, then $3 \times SO_3$ at ca. 910 °C). However, the subdivision of the respective steps is critical, since from the DTG curve further smaller maxima can be observed. From the TG curve these processes are hard to quantify as they overlap and no reliable intermediates can be distinguished. Therefore these steps have been merged into the two larger steps mentioned above. The decomposition process is finished at ca. 975 °C with the respective rare-earth niobates $RENbO_4$ (RE = Pr, Nd) as product.

For the samarium compound a different thermal behavior can be observed. The decomposition starts with the loss of a molecule of H_2O and SO_3 at 573 °C. This is understandable from the perspective of the increasing dehydration temperature also observed for the praseodymium and the niobium compound due to the increase in strength of the hydrogen bridge in the [$H(SO_4)_2$] ion. Therefore dehydration takes place in one step together with the loss of one molecule of SO_3. The intermediate of the approximate composition $Sm_2Nb_2O_2(SO_4)_6$ is not stable over a wider temperature range, but loses three molecules of SO_3 beginning at ca. 630 °C. This process is finished at 760 °C and leaves a residue of the composition $Sm_2Nb_2O_5(SO_4)_3$ or more likely $Sm_2(SO_4)_3 + Nb_2O_5$. Beginning at 810 °C this intermediate loses the last three molecules of SO_3 leading to $SmNbO_4$ as product (finished at 948 °C).

A slightly different decomposition reaction is found for the respective gadolinium compound. It is analogous to $Sm_2Nb_2O_2(SO_4)_3[H(SO_4)_2]_2$ and a molecule of H_2O is split off in the first step beginning at 557 °C. However, dehydration is accompanied by the loss of two molecules of SO_3. The hypothetical product $Gd_2Nb_2O_4(SO_4)_5$ is not stable and loses two molecules of sulfur trioxide, which is completed at 770 °C. Most likely an intermediate of the composition $Gd_2Nb_2O_5(SO_4)_3$ or probably $Gd_2(SO_4)_3 + Nb_2O_5$ in analogy to the samarium compound is formed. Further heating leads to the loss of three molecules of SO_3 with the formation of $GdNbO_4$ in a similar temperature frame already observed for $Sm_2Nb_2O_2(SO_4)_3[H(SO_4)_2]_2$ (T_S = 802 °C, T_E = 928 °C).

Significant changes in the thermal decomposition behavior can be observed for the smaller rare-earth ions of Dy and Er. In agreement with the strong hydrogen bridge in the [$H(SO_4)_2$] ion found for the smaller RE^{3+} ions, the dehydration reaction is not involved in the first decomposition step. Instead, the disintegration starts with the loss of one molecule of SO_3 at 503 °C (Dy) or 415 °C (Er). The product of the formal constitution $RE_2Nb_2O_3(SO_4)_2[H(SO_4)_2]_2$ is rather stable, as the decomposition continues at ca. 580 °C for both compounds. For the dysprosium compound this involves the loss of a further molecule of SO_3 accompanied by the dehydration reaction. However, the intermediate of the composition $Dy_2Nb_2O_4(SO_4)_5$ is not stable and loses two further molecules of sulfur trioxide with the formation

 © 2011 Wiley-VCH Verlag GmbH & Co. KGaA, Weinheim

of $Dy_2Nb_2O_5(SO_4)_3$ or $Dy_2(SO_4)_3$ + Nb_2O_5. For the respective erbium compound the decomposition pathway is slightly different, since a small step at 623 °C can be observed where the loss of mass can be assigned to the dehydration reaction of $Er_2Nb_2O_3(SO_4)_2[H(SO_4)_2]_2$ with the formation of an intermediate of the formal composition $Er_2Nb_2O_3(SO_4)_6$. Further heating leads to the loss of three molecules of SO_3, which is complete at roughly 830 °C and leads to a residue of $Er_2Nb_2O_5(SO_4)_3$ or $Er_2(SO_4)_3$ + Nb_2O_5. For both the Dy and Er compound the last decomposition step involves the loss of three molecules of SO_3 at a similar temperature (T_S ca. 800–830 °C, T_E ca. 905–920 °C) leading to $RENbO_4$ as product.

The cerium compound $Ce_2Nb_2O_2(SO_4)_3[H(SO_4)_2]_2$ does not fit into this pattern. Despite the weaker hydrogen bond in the $[H(SO_4)_2]$ ion and the trends already observed for the neighbors Pr and Nd, the decomposition does not start with the dehydration reaction. Instead a significantly larger loss of mass can be observed, which is in perfect accord with the loss of one molecule of SO_3. As expected, the decomposition temperature is lower than that for the respective Pr and Nd compound (293 °C) and the cerium analog fits perfectly into the trend for the decomposition starting temperature observed for the complete series. However, the intermediate of the formal constitution $Ce_2Nb_2O_3(SO_4)_2$-$[H(SO_4)_2]_2$ is pretty stable, as the next decomposition step does not occur until 575 °C. In this step, which is finished roughly at 760 °C, a water molecule as well as three molecules of SO_3 are split off leading to $Ce_2Nb_2O_5(SO_4)_3$ or $Ce_2(SO_4)_3$ + Nb_2O_5. In the final step, which is finished at 900 °C, the last three molecules of sulfur trioxide are lost with the formation of $CeNbO_4$.

$Bi_2Nb_4O_5(SO_4)_8$ decomposes in one step beginning at 552 °C with a loss of eight molecules of sulfur trioxide according to the observed loss of mass. The decomposition process is finished at 755 °C and leads to a product of the formal composition $Bi_2Nb_4O_9$. The residue has been investigated by X-ray powder diffraction. From the powder pattern triclinic $BiNbO_4$ can be identified without any doubt. However, the powder diagram exhibits several weak reflections, which can not be assigned to bismuth niobate. Most likely they are caused by Nb_2O_5 of poor crystallinity.

Discussion and Conclusion

In the crystal structures of the ternary rare-earth refractory metal sulfates presented in this work some similarities to the simple binary oxide sulfates of these elements as well as significant differences among this class of compounds can be observed.

The first is the tendency to include oxide ions into the crystal structures, which is also ubiquitous of other compounds containing high-valent metals, and is not exclusively limited to complex oxo anions. These oxido ligands are able to reduce the high effective positive charge on the metal by additional electron donation. Furthermore, the inclusion of oxido ligands into the coordination sphere of a high-valent metal leads to significant distortion effects for the coordination polyhedron around the metal. This effect is also present in the ternary sulfates presented here, and is manifested for example in the large variation in the M–O bond distances. For the bonding between metal and oxide ions two theories have been established, both deliver an explanation of the resulting distortion effects.

For compounds of a more or less molecular nature the model of the structural *trans* effect is commonly used. The bond between the metal and oxygen atom is described as a multiple bond composed of M–O σ-bonding and additional π-donation from the oxido ligand towards the metal.[20,21] This is in good accord with the usually very short M–O bond distances of 155 to 180 pm found for this class of compounds. Because of the competition for the same metal orbital the π-donation from the oxide ion towards the metal leads to a weakening and therefore a lengthening of the bond to the ligand in the *trans* position towards the [M=O] moiety, an effect which is sometimes referred to as *trans* lengthening.[22,23]

A second model explaining the distortion effects around high-valent transition-metal ions originates from the solid-state chemistry of these elements. The distortion effects are not discussed from the perspective of one single metal and oxide ion with their discrete molecular orbitals, but from a larger number of atoms assuming a band model. The metal ions are displaced inside their coordination polyhedra according to a second order Jahn–Teller effect. This displacement allows the mixing of empty metal d orbitals with filled p orbitals of the ligands enabling the reduction of the effective positive charge on the metal ion.[24–27] This theorem is of great importance for nonlinear optical effects, and has been studied intensively with a special focus on binary and ternary oxides of d^0 ions.[28]

For the binary refractory metal sulfates the decision on which theory is applicable for explaining the observed distortion effects has been ambiguous, as these compounds are polymers and not of a molecular nature.[11] However, they exhibit discrete [M=O] moieties featuring a bonding situation normally found for molecular complexes of these elements. Therefore, these compounds lie on the borderline between the molecular model of the structural *trans* effect and the second order Jahn–Teller distortions. Both models give possible explanations of the degree and direction of the distortions.

For the ternary rare-earth refractory metal oxide sulfates the situation is somewhat different. On the one hand RE_2-$[W_2O_3(SO_4)_6]$ (RE = Sm–Gd, Ho) and $Sm_2Nb_2O_2(SO_4)_5$-(S_2O_7) exhibit a similar bonding situation to the binary oxide sulfates of the refractory elements, as they contain discrete [M=O] moieties and comparable distortion effects around the metal ion. This is especially the case for $Sm_2Nb_2O_2(SO_4)_5(S_2O_7)$, which exhibits similar refractory metal-containing layers like in $MoO(HSO_4)(SO_4)$ or $WO(SO_4)_2$ for example. Therefore these types of compounds should also be considered as a borderline case between a structural *trans* effect and second order Jahn–Teller distortions.

 © 2011 Wiley-VCH Verlag GmbH & Co. KGaA, Weinheim

On the other hand, for $RE_2Nb_2O_2(SO_4)_3[H(SO_4)_2]_2$ (RE = Y, Ce–Nd, Sm–Er) and especially $M_2Nb_4O_5(SO_4)_8$ (M = Bi, Eu) the situation is different, as in these compounds no discrete [M=O] moieties featuring a terminal oxido ligand are found. Therefore, the model of the structural *trans* effect is not of good applicability here. The oxide ions bridge rare-earth and refractory metal ions, which is clearly visible in the elongation of the respective RM=O bond (RM = refractory metal). These asymmetric M=O···M bridges are a typical consequence of a second order Jahn–Teller effect.[29] Therefore the ternary rare-earth refractory metal sulfates deliver nice examples for the discussion of distortion effects around high-valent transition metals.

A significant influence on the characteristics of the [M=O] moieties in the compounds formed can be attributed to the synthesis conditions. The most important role with regard to this is the SO_3 content of the sulfuric acid, which is nicely illustrated in the comparison of the structures of $RE_2Nb_2O_2(SO_4)_3[H(SO_4)_2]_2$ (RE = Y, Ce–Nd, Sm–Er) and $Sm_2Nb_2O_2(SO_4)_5(S_2O_7)$. Both can be prepared from equimolar mixtures of Nb and RE, but the latter is obtained from sulfuric acid containing 25% SO_3, while the former can only be crystallized from water free H_2SO_4 containing no SO_3 excess.

The thermal behavior turned out to be a very interesting property of the ternary rare-earth refractory metal sulfates. This is especially the case for $RE_2Nb_2O_2(SO_4)_3[H(SO_4)_2]_2$ (RE = Y, Ce–Nd, Sm–Er), where the thermal behavior could be determined for various compounds of the complete range of RE^{3+} ionic radii between Ce and Er. Here a significant advantage of the rare-earth ions in contrast to other metal ions as ternary component (alkaline metals for example) becomes apparent, as they are able to build isostructural compounds whose properties are tunable by the radius of the respective rare-earth ion. This fact is nicely illustrated for both the influence of RE^{3+} on the decomposition temperature of $RE_2Nb_2O_2(SO_4)_3[H(SO_4)_2]_2$ (RE = Y, Ce–Nd, Sm–Er) and also the decomposition mechanism. Therefore, by a mere variation of the radius of RE^{3+} the decomposition mechanism can be altered in different directions enabling the generation of various intermediate phases. However, it should be noted that the isolation and especially the structural analysis of such decomposition intermediates is difficult, as the temperature frame in which these compounds are stable is usually small.

As a first success the possible intermediate of the dehydration reaction of $RE_2Nb_2O_2(SO_4)_3[H(SO_4)_2]_2$ (RE = Y, Ce–Nd, Sm–Er) leading most likely to a disulfate, could be obtained for $Sm_2Nb_2O_2(SO_4)_5(S_2O_7)$. However, the final proof, that the dehydration product adopts the structure found for $Sm_2Nb_2O_2(SO_4)_5(S_2O_7)$ could not be provided.

Experimental Section

Synthesis: All reactions were carried out using commercial fuming sulfuric acid containing 65% dissolved SO_3 (puriss., Merck, Darmstadt, Germany). If a lower sulfur trioxide content was necessary, the 65% oleum was diluted with the calculated amount of commercial 95–98% sulfuric acid (pure, BüFa, Oldenburg Germany) to the desired content of sulfur trioxide.

$RE_2[W_2O_3(SO_4)_6]$ (RE = Sm–Gd, Ho): A mixture of $WOCl_4$ (0.25 g) and the corresponding rare-earth oxide (99.9%, Chempur, Karlsruhe, Germany) in a molar ratio of W/RE = 1:1 was loaded into a thick-walled glass ampoule (25 cm in length and 2 cm in diameter). After addition of oleum (2 mL) containing 25% SO_3 the ampoule was torch-sealed, placed in a block thermostat (Gefran 800P, Liebisch, Bielefeld, Germany), and heated to 310 °C. The temperature was maintained for 3 d and finally slowly decreased to room temperature at a rate of 2 °C/h. The ampoule was opened in a glove box under an inert atmosphere, and the mother liquor was separated from the crystals by decantation. The last traces of adhesive sulfuric acid were removed by washing the crystals with absolute ethyl acetate, followed by drying in vacuo. In most cases, besides $RE_2[W_2O_3(SO_4)_6]$, the formation of rare-earth hydrogensulfate disulfates $RE(HSO_4)(S_2O_7)$ were observed,[30,31] which could be distinguished (comparatively large polyhedra) from the needle-shaped crystals of $RE_2[W_2O_3(SO_4)_6]$. Only the europium compound could be prepared free of $Eu(HSO_4)(S_2O_7)$, so that its thermal decomposition could be examined.

The reactant $WOCl_4$ was prepared according to literature methods by heating a suspension of WO_3 (99.8%, Alfa-Aesar, Karlsruhe, Germany) in thionyl chloride to 200 °C in a sealed glass ampoule for 8 h.[32] After evaporation to dryness the $WOCl_4$ was purified through sublimation under reduced pressure.

$RE_2Nb_2O_2(SO_4)_3[H(SO_4)_2]_2$ (RE = Y, Ce–Nd, Sm–Er): A mixture of $NbCl_5$ (0.25 g) (99%, Alfa-Aesar, Karlsruhe, Germany) and the corresponding rare-earth oxide in a molar ratio of Nb/RE = 1:1 was loaded into a glass ampoule. After addition of 100% H_2SO_4 (2 mL), which was prepared by adding the stoichiometric amount of SO_3 in the form of 65% oleum to commercial 95% H_2SO_4, the ampoule was torch-sealed and heated to 300 °C for 3 d in a block thermostat and finally cooled to room temperature (2 °C/h). After removing the mother liquor by decantation under an inert atmosphere, the crystals were washed with absolute ethyl acetate and dried in vacuo to remove all the remaining sulfuric acid. $RE_2Nb_2O_2(SO_4)_3[H(SO_4)_2]_2$ formed pyramidal crystals, which grew to a respectable size for the middle sized RE^{3+} ions of Sm, Eu, and Gd. With a decreasing radius of RE^{3+} the crystals became smaller and exhibited a tendency towards twinning. For the larger cations Ce^{3+} and Pr^{3+} the formation of a microcrystalline side product of unknown constitution was observed, which could be separated from the crystals of $RE_2Nb_2O_2(SO_4)_3[H(SO_4)_2]_2$ during the washing process with ethyl acetate. For the rare-earth ions smaller than Er^{3+} the hydrogensulfate disulfates $RE(HSO_4)(S_2O_7)$ were formed instead of $RE_2Nb_2O_2(SO_4)_3[H(SO_4)_2]_2$. When commercial 95% H_2SO_4 was used, the rare-earth hydrogensulfates $RE(HSO_4)_3$ were the main product (hexagonal needles of respectable length).[33]

$Sm_2Nb_2O_2(SO_4)_5(S_2O_7)$: A mixture of $NbCl_5$ (0.25 g) and the equimolar amount of $Sm(NO_3)_3{\cdot}6H_2O$ was placed into a glass ampoule. After adding oleum (2 mL) containing 25% SO_3 the ampoule was torch-sealed and heated to 310 °C in a block thermostat for 3 d. After slow cooling to room temperature (2 °C/h) numerous polyhedral crystals of $Sm(HSO_4)(S_2O_7)$ together with a few needles of $Sm_2Nb_2O_2(SO_4)_5(S_2O_7)$ separated out. The needle shaped crystals of $Sm_2Nb_2O_2(SO_4)_5(S_2O_7)$ were isolated from $Sm(HSO_4)(S_2O_7)$ mechanically using an inert oil. Because of the small yield of the title compound only the crystal structure has been determined.

$M_2Nb_4O_5(SO_4)_8$ (M = Bi, Eu): A mixture of $NbCl_5$ (0.75 g) and $(BiO)_2CO_3$ (0.18 g) (99%, Alfa-Aesar, Karlsruhe, Germany) (Nb/Bi = 4:1) or $NbCl_5$ (0.25 g) and Eu_2O_3 (0.02 g) (Nb/Eu = 8:1) in

 © 2011 Wiley-VCH Verlag GmbH & Co. KGaA, Weinheim

95% H_2SO_4 (4 mL) was transferred into a glass ampoule and heated to 310 °C in a block thermostat for 3 days. After slow cooling to room temperature (2 °C/h) the respective bismuth compound was obtained as the only product in the form of comparatively long needles, which were freed from adherent sulfuric acid by washing with ethyl acetate and subsequent drying in vacuo. For the europium compound the crystallization of $Eu(HSO_4)_3$ was always observed, even if the amount of Eu_2O_3 was very small compared with $NbCl_5$. Therefore, the thermal decomposition has only been investigated for $Bi_2Nb_2O_5(SO_4)_8$.

Thermal Analysis: The sample (10–20 mg) was placed in a corundum crucible in a glove box and transferred to a thermoanalyzer (TGA/SDTA 851^e, Mettler–Toledo, Schwerzenbach, Switzerland). The sample was heated at a constant rate of 10 °C/min under flowing nitrogen. The thermal decomposition was monitored from 25 °C up to 1050 °C. Characteristic points like onset and end temperatures of the thermal effects were taken from the differentiated DTA curve following common procedures using the software delivered with the analyzer.[34] Thermal decomposition data for the compounds presented in this work are summarized in Table 5.

Structure Determination: Some of the single crystals were selected from a protecting oil with the help of a polarization microscope. They were mounted onto a glass capillary tube and placed into the cold nitrogen stream (153 K) of a single crystal diffractometer (κ-APEX II, Bruker, Karlsruhe, Germany or IPDS-I, Stoe, Darmstadt, Germany). For the respective best specimen intensity data were collected. Atomic positions and further details of the crystal structure can be obtained from the Fachinformationszentrum Karlsruhe, 76344 Eggenstein-Leopoldshafen, Germany, on quoting the deposition number given in Tables 1 and 2.

$RE_2[W_2O_3(SO_4)_6]$ (RE = Sm–Gd, Ho): Inspection of systematic absences suggested the monoclinic space group *C*2/*c* and the structure solution assuming this space group was successful applying direct methods (SHELXS).[35] Subsequent refinement with the SHELXL program yielded the complete crystal structure.[36] After introduction of anisotropic displacement parameters a numerical absorption correction was applied to the reflection data using the programs X-RED and X-SHAPE.[37,38] However, the $[W_2O_3(SO_4)_6]^{6-}$ ion exhibited a disorder along [010], which could be refined successfully by splitting the position of the tungsten atom (W1), the terminal oxido ligand (O11), and the oxido bridge (O1). Table 1 gives details of the data collection and crystallographic data.

$RE_2Nb_2O_2(SO_4)_3[H(SO_4)_2]_2$ (RE = Y, Ce–Nd, Sm–Er): Structure solution was easily possible in the tetragonal space group $P\bar{4}2_1m$ using the direct methods of the SHELXS program. During the refinement process with SHELXL all missing non-hydrogen atoms were found from a Fourier map. After introducing anisotropic displacement parameters and application of a numerical absorption correction the structures refined to the quality criteria given in Table 2. The correct absolute structure is indicated by the Flack-X parameter of around zero for all compounds. The position of the hydrogen atom of the hydrogen bis(sulfate) group could not be determined, most likely because of the double minimum potential found for the H atom in these strong hydrogen bridge bonds.

$Sm_2Nb_2O_2(SO_4)_5(S_2O_7)$: The structure was easily solved in the monoclinic space group *I*2/*a* using the direct methods of the SHELXS program. All missing atoms were found from a Fourier map during subsequent refinement with SHELXL. Anisotropic displacement parameters were introduced and a numerical absorption correction (X-RED, X-SHAPE) was applied to the data. Details on the data collection and crystallographic data are given in Table 3.

$M_2Nb_2O_5(SO_4)_8$ (M = Bi, Eu): Initially, unit cell determination using reflections of a reasonable intensity [$I > 10\sigma(I)$] lead to a *C*-centered monoclinic cell [e.g. for M = Bi: a = 1624.57(5) pm, b = 816.00(2) pm, c = 2208.13(6) pm, β = 111.089(1)°, V = 2.7312(2) nm^3]. Structure solution and refinement in space group *C*2/*c* using the SHELXS/SHELXL programs was uncomplicated, but nearly all oxygen atoms exhibited a disorder over two equally occupied positions. As this disordered model was chemically implausible for the highly networking sulfate ions in this structure, the diffraction images were reinvestigated. Various weak reflections were found, which were not indexed with the above-mentioned unit cell. Therefore the unit cell determination was repeated with a special focus on these weaker reflections, which lead to a similar monoclinic *C*-centered cell with a doubled *a* and *b* axis. Structure solution and refinement assuming this unit cell of fourfold volume was uncomplicated and lead to a model without disorder. However, as the positions of the Bi and Nb atoms – and to a certain extent the sulfur atoms too – were refinable using the smaller unit cell, correlations between their atom coordinates could be found. Never-

Table 1. Crystallographic data for $RE_2W_2O_3(SO_4)_6$ (RE = Sm, Eu, Gd, Ho).

Empirical formula	$Sm_2W_2O_3(SO_4)_6$	$Eu_2W_2O_3(SO_4)_6$	$Gd_2W_2O_3(SO_4)_6$	$Ho_2W_2O_3(SO_4)_6$
M_r [g/mol]	1292.76	1295.98	1306.56	1321.92
a [pm]	2000.93(5)	2002.3(2)	2006.5(2)	2001.8(2)
b [pm]	554.35(1)	552.13(4)	550.49(5)	542.66(3)
c [pm]	1868.91(5)	1869.5(2)	1866.2(2)	1851.2(2)
β [°]	100.923(1)	100.77(1)	100.81(2)	100.68(1)
V [nm^3]	2.03547(8)	2.0304(3)	2.0247(4)	1.9761(3)
Z	4	4	4	4
Space group	*C*2/*c* (No. 15)	*C*2/*c* (No. 15)	*C*2/*c* (No. 15)	*C*2/*c* (No. 15)
T [°C]	–120	–120	–120	–120
λ [pm]	71.073	71.073	71.073	71.073
D_{calcd} [g/cm^3]	4.219	4.240	4.286	4.443
μ [cm^{-1}]	177.00	181.38	185.45	202.96
R_1[a] [$F_o > 2\sigma(F_o)$]	0.0201	0.0437	0.0417	0.0265
wR_2[b] [$F_o > 2\sigma(F_o)$]	0.0526	0.0796	0.0988	0.0601
R_1[a] (all data)	0.0232	0.0481	0.0635	0.0372
wR_2[b] (all data)	0.0533	0.0837	0.1022	0.0621
Split model occupation	0.90/0.10	0.94/0.06	0.84/0.16	0.83/0.17
CSD number	423206	423204	423205	423207

[a] R_1 is defined as $\Sigma||F_o| - |F_c||/\Sigma|F_o|$ for $I > 2\sigma(I)$. [b] wR_2 is defined as $\{\Sigma[w(F_o^2 - F_c^2)^2] / \Sigma[w(F_o^2)^2]\}^{1/2}$.

 © 2011 Wiley-VCH Verlag GmbH & Co. KGaA, Weinheim

Table 2. Crystallographic data for $RE_2Nb_2O_2(SO_4)_3[H(SO_4)_2]_2$ (RE = Y, Ce–Nd, Sm–Er).

Empirical formula	$Ce_2Nb_2O_2(SO_4)_3$-$[H(SO_4)_2]_2$	$Pr_2Nb_2O_2(SO_4)_3$-$[H(SO_4)_2]_2$	$Nd_2Nb_2O_2(SO_4)_3$-$[H(SO_4)_2]_2$	$Sm_2Nb_2O_2(SO_4)_3$-$[H(SO_4)_2]_2$	$Eu_2Nb_2O_2(SO_4)_3$-$[H(SO_4)_2]_2$	$Gd_2Nb_2O_2(SO_4)_3$-$[H(SO_4)_2]_2$
M_r [g/mol]	1172.50	1174.08	1180.74	1192.96	1196.18	1206.76
a [pm]	1282.59(7)	1277.79(8)	1275.0(1)	1269.87(4)	1269.09(6)	1267.79(8)
c [pm]	722.04(5)	717.33(4)	715.03(6)	709.70(2)	709.47(4)	708.18(7)
V [nm^3]	1.1878(2)	1.1712(2)	1.1607(2)	1.14444(6)	1.1427(1)	1.1383(2)
Z	2	2	2	2	2	2
Space group	$P\bar{4}2_1m$ (No. 113)	$P\bar{4}2_1m$ (No. 113)	$P\bar{4}2_1m$ (No. 113)	$P\bar{4}2_1m$ (No. 113)	$P\bar{4}2_1m$ (No. 113)	$P\bar{4}2_1m$ (No. 113)
T [°C]	–120	–120	–120	–120	–120	–120
λ [pm]	71.073	71.073	71.073	71.073	71.073	71.073
D_{calcd} [g/cm^3]	3.278	3.329	3.378	3.462	3.477	3.521
μ [cm^{-1}]	54.49	57.99	61.27	68.09	71.69	75.13
R_1[a] [$F_O > 2\sigma(F_O)$]	0.0249	0.0142	0.0190	0.0148	0.0280	0.0307
wR_2[b] [$F_O > 2\sigma(F_O)$]	0.0597	0.0340	0.0376	0.0361	0.0684	0.0635
R_1[a] (all data)	0.0263	0.0144	0.0207	0.0148	0.0289	0.0361
wR_2[b] (all data)	0.0602	0.0341	0.0379	0.0361	0.0687	0.0646
Flack-X parameter	–0.01(2)	0.001(5)	–0.009(6)	0.006(7)	0.01(2)	–0.02(2)
CSD Number	423208	423209	423210	423211	423212	423213

Empirical formula	$Tb_2Nb_2O_2(SO_4)_3$-$[H(SO_4)_2]_2$	$Dy_2Nb_2O_2(SO_4)_3$-$[H(SO_4)_2]_2$	$Ho_2Nb_2O_2(SO_4)_3$-$[H(SO_4)_2]_2$	$Er_2Nb_2O_2(SO_4)_3$-$[H(SO_4)_2]_2$	$Y_2Nb_2O_2(SO_4)_3$-$[H(SO_4)_2]_2$
M_r [g/mol]	1210.10	1217.26	1222.12	1226.78	1206.76
a [pm]	1263.67(2)	1264.07(8)	1261.90(8)	1257.29(3)	1267.79(8)
c [pm]	704.38(1)	703.15(5)	702.18(7)	698.61(2)	708.18(7)
V [nm^3]	1.12480(3)	1.1235(2)	1.1182(2)	1.10435(4)	1.1383(2)
Z	2	2	2	2	2
Space group	$P\bar{4}2_1m$ (No. 113)	$P\bar{4}2_1m$ (No. 113)	$P\bar{4}2_1m$ (No. 113)	$P\bar{4}2_1m$ (No. 113)	$P\bar{4}2_1m$ (No. 113)
T [°C]	–120	–120	–120	–120	–120
λ [pm]	71.073	71.073	71.073	71.073	71.073
D_{calcd} [g/cm^3]	3.573	3.598	3.630	3.689	3.521
μ [cm^{-1}]	79.94	83.59	87.93	93.38	75.13
R_1[a] [$F_O > 2\sigma(F_O)$]	0.0184	0.0282	0.0288	0.0152	0.0307
wR_2[b] [$F_O > 2\sigma(F_O)$]	0.0291	0.0597	0.0603	0.0375	0.0635
R_1[a] (all data)	0.0211	0.0334	0.0340	0.0152	0.0361
wR_2[b] (all data)	0.0295	0.0606	0.0618	0.0375	0.0646
Flack-X parameter	–0.015(6)	–0.03(2)	–0.04(2)	0.003(5)	–0.40(8)
CSD Number	423214	423215	423216	423217	423219

[a] R_1 is defined as $\sum||F_o| - |F_c||/\sum|F_o|$ for $I > 2\sigma(I)$. [b] wR_2 is defined as $\{\sum[w(F_o^2 - F_c^2)^2]/\sum[w(F_o^{2)2}]\}^{1/2}$.

Table 3. Crystallographic data for $Sm_2Nb_2O_2(SO_4)_5(S_2O_7)$.

Empirical formula	$Sm_2Nb_2O_2(SO_4)_5(S_2O_7)$
M_r [g/mol]	1174.94
a [pm]	916.79(6)
b [pm]	883.04(7)
c [pm]	2760.9(2)
β [deg]	93.976(8)
V [nm^3]	2.2297(3)
Z	4
Space group	$I2/a$ (No. 15)
T [°C]	–120
λ [pm]	71.073
D_{calcd} [g/cm^3]	3.500
μ [cm^{-1}]	69.83
R_1[a] [$F_o > 2\sigma(F_o)$]	0.0196
wR_2[b] [$F_o > 2\sigma(F_o)$]	0.0341
R_1[a] (all data)	0.0316
wR_2[b] (all data)	0.0352
CSD Number	423218

[a] R_1 is defined as $\sum||F_o| - |F_c||/\sum|F_o|$ for $I > 2\sigma(I)$. [b] wR_2 is defined as $\{\sum[w(F_o^2 - F_c^2)^2]/\sum[w(F_o^{2)2}]\}^{1/2}$.

Table 4. Crystallographic data for $M_2Nb_4O_5(SO_4)_8$ (M = Bi, Eu).

Empirical formula	$Bi_2Nb_4O_5(SO_4)_8$	$Eu_2Nb_4O_5(SO_4)_8$
M_r [g/mol]	1638.08	1524.04
a [pm]	3249.05(9)	3248.4(2)
b [pm]	1632.02(5)	1634.94(6)
c [pm]	2208.21(6)	2206.79(9)
β [deg]	111.087(1)	111.213(2)
V [nm^3]	10.9250(5)	10.9260(7)
Z	16	16
Space group	$C2/c$ (No. 15)	$C2/c$ (No. 15)
T [°C]	–120	–120
λ [pm]	71.073	71.073
D_{calcd} [g/cm^3]	3.984	3.706
μ [cm^{-1}]	152.28	69.09
R_1[a] [$F_O > 2\sigma(F_O)$]	0.0247	0.0331
wR_2[b] [$F_O > 2\sigma(F_O)$]	0.0437	0.0694
R_1[a] (all data)	0.0686	0.0788
wR_2[b] (all data)	0.0494	0.0788
CSD Number	423202	423203

[a] R_1 is defined as $\sum||F_o| - |F_c||/\sum|F_o|$ for $I > 2\sigma(I)$. [b] wR_2 is defined as $\{\sum[w(F_o^2 - F_c^2)^2]/\sum[w(F_o^{2)2}]\}^{1/2}$.

theless, the structure of the bismuth as well as the europium compound could be refined to satisfying residual values. Details on the data collection and crystallographic data are given in Table 4.

Powder Diffraction: X-ray powder diffraction investigations were performed with the help of the powder diffractometer STADI-P (Stoe, Darmstadt, Germany) using Cu-$K_{\alpha1}$ radiation and a flat

 © 2011 Wiley-VCH Verlag GmbH & Co. KGaA, Weinheim

Table 5. Thermal decomposition data for $Eu_2[W_2O_3(SO_4)_6]$ and $RE_2Nb_2O_2(SO_4)_3[H(SO_4)_2]_2$ (RE = Ce–Er, Y).[a]

	Step	T_S [°C]	T_{max} [°C]	T_E [°C]	Reaction	Δm_{exp} [%]	Δm_{calc} [%]	Product
$Ce_2Nb_2O_2(SO_4)_3[H(SO_4)_2]_2$	1	293	332	340	$-SO_3$	6.8	6.8	
	2	575	646	≈760	$-3SO_3$, $-H_2O$	27.7	28.8	
	3	≈760	884	900	$-3SO_3$	49.3	49.3	$CeNbO_4$
$Pr_2Nb_2O_2(SO_4)_3[H(SO_4)_2]_2$	1	461	487	513	$-H_2O$	1.5	1.5	
	2	560	675	≈760	$-4SO_3$	28.5	28.8	
	3	≈800	920	980	$-3SO_3$	48.8	49.3	$PrNbO_4$
$Nd_2Nb_2O_2(SO_4)_3[H(SO_4)_2]_2$	1	500	527	545	$-H_2O$	1.6	1.5	
	2	560	683	760	$-4SO_3$	28.8	28.6	
	3	805	907	971	$-3SO_3$	49.1	48.9	$NdNbO_4$
$Sm_2Nb_2O_2(SO_4)_3[H(SO_4)_2]_2$	1	573	611	≈630	$-SO_3$, $-H_2O$	8.4	8.2	
	2	≈630	696	760	$-3SO_3$	28.4	28.3	
	3	810	890	948	$-3SO_3$	48.1	48.4	$SmNbO_4$
$Gd_2Nb_2O_2(SO_4)_3[H(SO_4)_2]_2$	1	557	597	≈670	$-2SO_3$, $-H_2O$	12.9	14.7	
	2	≈670	716	770	$-2SO_3$	27.8	28.0	
	3	802	876	928	$-3SO_3$	47.8	47.9	$GdNbO_4$
$Dy_2Nb_2O_2(SO_4)_3[H(SO_4)_2]_2$	1	503	527	≈580	$-SO_3$	6.0	6.6	
	2	≈580	631	≈680	$-SO_3$, $-H_2O$	13.3	14.6	
	3	≈680	731	790	$-2SO_3$	27.6	27.8	
	4	800	867	905	$-3SO_3$	47.2	47.5	$DyNbO_4$
$Er_2Nb_2O_2(SO_4)_3[H(SO_4)_2]_2$	1	415	456	510	$-SO_3$	5.9	6.5	
	2	≈580	623	≈660	$-H_2O$	7.6	8.0	
	3	≈670	795	≈830	$-3SO_3$	27.3	27.5	
	4	≈830	879	920	$-3SO_3$	46.0	47.1	$ErNbO_4$
$Bi_2Nb_4O_5(SO_4)_8$	1	552	662	755	$-8SO_3$	38.8	39.1	$2BiNbO_4/Nb_2O_5$
$Eu_2[W_2O_3(SO_4)_6]$	1	≈230	272	≈300	vap. H_2SO_4	1.9	–	
	2	340	375	405	$-SO_3$	6.3	6.2	
	3	543	594	634	$-2SO_3$	19.5	18.5	
	4	≈700	904	943	$-3SO_3$	39.6	37.0	$Eu_2W_2O_9$

[a] T_S: Starting temperature of the thermal decomposition; T_{max}: Maximum of the first derivative of the TG curve; T_E: Temperature at which the thermal decomposition has finished.

sample holder. The data were processed with the software delivered with the diffractometer.[39]

Supporting Information (see footnote on the first page of this article): Plots of the thermal decomposition data for $Eu_2[W_2O_3(SO_4)_6]$, $RE_2Nb_2O_2(SO_4)_3[H(SO_4)_2]_2$, and $Bi_2Nb_4O_5(SO_4)_8$ (TG and DTG curve) as well as X-ray powder patterns of the respective residues.

Acknowledgments

The authors thank Mr. Wolfgang Saak for the collection of the X-ray data. We also thank the Fonds der Chemischen Industrie and the Heinz-Neumüller-Stiftung for granting a stipend to U. B. Funding through the Deutsche Forschungsgemeinschaft (DFG) is gratefully acknowledged.

[1] S. S. Pollack, *Inorg. Chem.* **1987**, *26*, 1825–1826.
[2] A. A. Kashaev, G. V. Sokolova, *Sov. Phys. Crystallogr.* **1973**, *18*, 388–389.
[3] J. Fuchs, H. U. Kreusler, A. Foerster, *Z. Naturforsch. B: Chem. Sci.* **1979**, *34*, 1683–1685.
[4] T. Noerbygaard, R. W. Berg, K. Nielsen, *Electrochem. Soc. Proc.* **1998**, *98*, 553–573.
[5] S. J. Cline Schäffer, R. W. Berg, *Acta Crystallogr., Sect. E Struct. Rep. Online* **2008**, *64*, i73.
[6] S. J. Cline Schäffer, R. W. Berg, *Acta Crystallogr., Sect. E Struct. Rep. Online* **2008**, *64*, i20.
[7] S. J. Cline Schäffer, R. W. Berg, *Acta Crystallogr., Sect. E Struct. Rep. Online* **2005**, *61*, i49–i51, 000–000.
[8] K. Ståhl, R. W. Berg, *Acta Crystallogr., Sect. E Struct. Rep. Online* **2009**, *65*, i88.
[9] F. Borup, R. W. Berg, K. Nielsen, *Acta Chem. Scand.* **1990**, *44*, 328–331.
[10] V. Y. Kuznetsov, D. L. Rogachev, L. M. Dikareva, M. A. Porai-Koshits, *J. Struct. Chem.* **1980**, *20*, 569–573
[11] U. Betke, M. S. Wickleder, *Inorg. Chem.* **2011**, *50*, 858–872.
[12] K.-L. Richter, R. Mattes, *Z. Anorg. Allg. Chem.* **1992**, *611*, 158–164.
[13] S. M. Islam, R. Glaum, *Z. Anorg. Allg. Chem.* **2009**, *635*, 1008–1013.
[14] M. Hanawa, H. Imoto, *J. Solid State Chem.* **1999**, *144*, 325–329.
[15] E. Kemnitz, C. Werner, S. Trojanov, *Acta Crystallogr., Sect. C: Cryst. Struct. Commun.* **1996**, *52*, 2665–2668.
[16] S. Fortier, M. E. Fraser, R. D. Heyding, *Acta Crystallogr., Sect. C: Cryst. Struct. Commun.* **1985**, *41*, 1139–1141.
[17] Y. Laligant, A. Le Bail, F. Goutenoire, *J. Solid State Chem.* **2001**, *159*, 223–227.
[18] S. V. Borisov, R. F. Klevtsova, *Kristallografiya* **1970**, *15*, 38–42.
[19] A. F. Holleman, N. Wiberg: *Lehrbuch der Anorganischen Chemie*, 102nd ed., de Gruyter Berlin, Germany, **2007**.
[20] C. J. Ballhausen, H. B. Gray, *Inorg. Chem.* **1962**, *1*, 111–122.
[21] H. B. Gray, C. R. Hare, *Inorg. Chem.* **1962**, *1*, 363–368.
[22] E. M. Shustorovich, M. A. Porai-Koshits, Y. A. Buslaev, *Coord. Chem. Rev.* **1975**, *17*, 1–98.
[23] B. J. Coe, S. J. Glenwright, *Coord. Chem. Rev.* **2000**, *203*, 5–80.
[24] M. Kunz, I. D. Brown, *J. Solid State Chem.* **1995**, *115*, 395–406.
[25] U. Öpik, M. H. L. Pryce, *Proc. R. Soc. London Ser. A* **1957**, *238*, 425–447.
[26] R. G. Pearson, *J. Am. Chem. Soc.* **1969**, *91*, 4947–4955.
[27] R. G. Pearson, *J. Mol. Struct.: THEOCHEM* **1983**, *103*, 25–34.

 © 2011 Wiley-VCH Verlag GmbH & Co. KGaA, Weinheim

[28] K. M. Ok, D. Casanova, M. Llunell, P. Alemany, S. Alvarez, P. S. Halasyamani, *Chem. Mater.* **2006**, *18*, 3176–3183.
[29] R. A. Wheeler, M.-H. Whangbo, T. Hughbanks, R. Hoffmann, J. K. Burdett, T. A. Albright, *J. Am. Chem. Soc.* **1986**, *108*, 2222–2236.
[30] M. S. Wickleder, *Z. Anorg. Allg. Chem.* **2000**, *626*, 621–622.
[31] S. Schwarzer, *Neuartige Sulfate der Platin- und Selten-Erd-Metalle*, Dissertation, University of Oldenburg, **2010**.
[32] H. Hecht, G. Jander, H. Schlapmann, *Z. Anorg. Chem.* **1947**, *254*, 255–264.
[33] M. S. Wickleder, *Z. Anorg. Allg. Chem.* **1998**, *624*, 1583–1587.
[34] *STAR*^{e}, version 8.1, *Controlling Program for the TGA/SDTA851*^{e} *Apparatus*, Mettler–Toledo GmbH, Schwerzenbach, Switzerland, **2004**.
[35] G. M. Sheldrick, *SHELXS-97*, *Program for the Solution of Crystal Structures*, University of Göttingen, Germany, **1997**.
[36] G. M. Sheldrick, *SHELXL-97*, *Program for the Refinement of Crystal Structures*, University of Göttingen, Germany, **1997**.
[37] *X-RED*, version 1.22, *Data Reduction for STADI4 and IPDS*, Stoe & Cie, Darmstadt, Germany, **2001**.
[38] *X-SHAPE*, version 1.06f, *Crystal Optimization for Numerical Absorption Corrections*, Stoe & Cie, Darmstadt, Germany, **1999**.
[39] *Win XPOW 2007*, *Software Package for the STOE Powder Diffraction System*, Stoe & Cie, Darmstadt, Germany, **2006**.

Received: June 22, 2011
Published Online: September 1, 2011

 © 2011 Wiley-VCH Verlag GmbH & Co. KGaA, Weinheim